The Astrophysical Journal, 978:23 (9pp), 2025 January 01 https://doi.org/10.3847/1538-4357/ad85d1

Central versus Global Quenching Traced by the APEX-CALIFA Survey

J. K. Barrera-Ballesteros[1], I. Cruz-González[1], D. Colombo[2], S. F. Sánchez[1], R. C. Levy[3,6], V. Villanueva[4], T. Wong[5], A. Bolatto[4], and D. Alonso Hernández[1]
[1] Universidad Nacional Autónoma de México, Instituto de Astronomía, AP 70-264, CDMX 04510, Mexico
[2] Max-Planck-Institut für Radioastronomie, Auf dem Hügel 69, 53121 Bonn, Germany
[3] Steward Observatory, University of Arizona, Tucson, AZ 85721, USA
[4] Department of Astronomy, University of Maryland, College Park, MD 20742, USA
[5] Department of Astronomy, University of Illinois, Urbana, IL 61801, USA
Received 2023 January 5; revised 2024 October 2; accepted 2024 October 7; published 2024 December 23

Abstract

The quest for the mechanisms that halt star formation in galaxies is essential to understand their evolution. Here, we use the APEX-CALIFA survey, which includes 560 galaxies ($0.005 < z < 0.08$), so far the largest sample of galaxies in the nearby universe with both Integral Field Spectroscopic, Calar Alto Legacy Integral Field Area (CALIFA) and single-aperture millimeter observations, as well as the extended CALIFA sample (823 targets). Using these observations we derive (i) the deficit or excess of star formation for a given stellar mass with respect to the star formation main sequence (ΔSFMS), (ii) the gas fraction, and (iii) the star formation efficiency (SFE) for two apertures (central and global apertures using the APEX-CALIFA and CALIFA samples, respectively). We confirm the so-called "inside-out" quenching, that is, for quiescent galaxies the central values of ΔSFMS are usually smaller than those values derived from global measurements. However, for a given ΔSFMS we find that for retired galaxies the central gas fraction is larger in comparison to global measurements. Furthermore, the central SFE is significantly smaller in comparison to global counterparts. In general, in comparison to the global measurements, the deficit of star formation at the center of retired galaxies is primarily caused by the inefficiency to form new stars rather than the lack of molecular gas. We suggest that even though at the center of retired galaxies the gas fraction is larger, morphological structures could prevent that the molecular gas is transformed into new stars. Even more so in the outskirts of some retired galaxies with small gas fractions, star formation activity is still occurring.

Unified Astronomy Thesaurus concepts: Red sequence galaxies (1373); Galaxy quenching (2040); Star formation (1569); Molecular gas (1073); Surveys (1671)

1. Introduction

Similar to the processes that trigger star formation in galaxies, those that halt the formation of new stars are of great relevance to understand how galaxies form and evolve. Thanks to spectrophotometric observations of large samples in the nearby Universe, we can describe galaxies according to their star formation activity. In a star formation rate–stellar mass (SFR–M_*) diagram a galaxy with a given stellar mass can be located either above, within, or below the so-called star formation main sequence (SFMS). Thus, a galaxy can be considered as a starburst, star forming, and retired or quiescent one, respectively. The small number of galaxies that are between star forming and retired are known as green valley galaxies (J. Brinchmann et al. 2004). Furthermore, star-forming or retired galaxies have distinctive morphologies. Usually the process associated with moving disk-like, star-forming galaxies into red, spheroidal-like and "dead" galaxies in the SFR–M_* diagram is known as star formation quenching (e.g., E. Cameron et al. 2009; E. F. Bell et al. 2012; A. F. L. Bluck et al. 2014, 2016, 2019; P. Lang et al. 2014; C. M. B. Omand et al. 2014).

Generally speaking, there have been two scenarios that could explain the absence of star formation activity in galaxies. On the one hand, the lack of cold molecular gas—the raw material to form new stars—is the cause of such quenching (A. Dekel & J. Silk 1986). Different processes are thought to be responsible for the removal of cold molecular gas in galaxies of different masses: for low-mass galaxies their shallow potential allows stellar feedback to eject the cold gas, whereas for massive galaxies a more energetic process such as winds and outflows due to nuclear activity are the cause of gas ejection or heating (e.g., S. Veilleux et al. 2013, 2020). On the other hand, star formation ceases even when molecular gas is present, in other words, the efficiency to form new stars is significantly reduced. This scenario is usually called "morphological quenching" (M. Martig et al. 2009), because the quenching fraction of the early-type galaxies is higher than that of the late-type galaxies (e.g., C. Liu et al. 2019), and morphological structures such as bulges restrain the cold gas to collapse avoiding a necessary condition to form new stars. This is also related to the so-called "inside-out" quenching where galaxies still have significant star formation activity in their outskirts in comparison to their centers (e.g., R. S. de Jong & P. C. van der Kruit 1994; R. M. González Delgado et al. 2014; C. Catalán-Torrecilla et al. 2017; S. Zibetti et al. 2017; I. Breda et al. 2020; V. Kalinova et al. 2021). Recent explorations have shown that it is possible that other mechanisms, such as lack of inflows of cold gas to galaxies at early epochs of the Universe, could result in a quenched galaxy (e.g., K. E. Whitaker et al. 2021).

Naturally, to explore which scenario is responsible for quenching star formation in galaxies it is required to have measurements of the molecular gas in a large sample of

[6] NSF Astronomy and Astrophysics Postdoctoral Fellow.

galaxies in the nearby Universe. Despite this, with remarkable exceptions (e.g., K. Alatalo et al. 2013; A. Saintonge et al. 2017; D. Colombo et al. 2020), most of the surveys devoted to estimating the amount of cold gas in the nearby Universe are dedicated to measuring it mostly in star-forming galaxies. Usually the observables used to quantify the star formation activity (or lack thereof) are the specific star formation rate (sSFR, this is closely related to the residuals of the SFMS, ΔSFMS), the star formation efficiency (SFE), and the gas fraction. The SFE is parameterized as the ratio between the star formation rate and the molecular gas mass ($M_{\rm mol}$): $\rm SFE = SFR/M_{mol}$, whereas the amount of gas with respect to the stellar mass is measured using the molecular gas fraction ($F_{\rm mol} = M_{\rm mol}/M_*$). For star-forming galaxies (i.e., galaxies within the SFMS) these values are typically constant with little variation depending on parameters such as the stellar mass or morphology ($\rm SFE \sim 10^{-9}\,yr^{-1}$, $F_{\rm mol} \sim 10^{-1}$, respectively; e.g., A. K. Leroy et al. 2008; S. Díaz-García & J. H. Knapen 2020).

There has been significant efforts to measure the properties of the molecular gas in galaxies with optical observations using integral field spectroscopy (IFS). One of the IFS samples where this has been happening is the Calar Alto Legacy Integral Field Area (CALIFA) Survey (S. F. Sánchez et al. 2012). Using a large sample of CALIFA galaxies with homogeneous APEX observations, D. Colombo et al. (2020) found that the central properties of galaxies that depart from the SFMS cover a significant dynamical range in both SFE and gas fraction. Furthermore, they suggested that different mechanisms may drive the separation of a given galaxy with respect to this sequence. While the lack of molecular gas sets a quiescent galaxy below the SFMS, a higher SFE moves a retired galaxy closer to the so-called retired region. Despite this notable effort to quantify the main process responsible for the quenching, this study focused only on how the central SFE and gas fraction are correlated with the global (or integrated) departure of the SFR with respect to the SFMS. In this study we use an updated sample of central molecular gas observations with APEX and those estimations of the global molecular gas via the Balmer decrement (i.e., the Hα/Hβ ratio) for the entire CALIFA sample. Our aim is to explore how the star formation activity (or lack thereof) for galaxies in the nearby Universe is affected by their physical properties such as the gas fraction or the efficiency at those two different scales. Given the fact that galaxies are spatially resolved objects, such explorations are essential to further disentangle what is the main driver of the quenching of star formation in galaxies. This article is structured as follows: in Section 2 the eCALIFA survey IFS data and EDGE-CALIFA with new APEX molecular gas data and derived parameters are described, followed by results presented in Section 3, and ending with discussion and conclusions in Section 4.

2. Data and Analysis

The aim of this study is to explore how the star formation activity (or lack thereof) for galaxies in the nearby Universe is affected by their physical properties such as the gas fraction or the SFE at different scales. To achieve this, we use the sample of galaxies included in the latest version of the CALIFA survey (S. F. Sánchez et al. 2012). Besides the galaxies presented in previous releases of this survey (∼600 objects; e.g., R. García-Benito et al. 2015; S. F. Sánchez et al. 2016a), this larger sample includes also additional galaxies that have been observed using the same strategy as the CALIFA survey. In a nutshell, the eCALIFA galaxies have been selected so their optical extension (∼2–3 effective radius) is within the field of view (FoV) of the IFS instrument. This sample, with a total of 823 galaxies, is known as the extended CALIFA (eCALIFA) sample (E. A. D. Lacerda et al. 2020; P. Alvarez-Hurtado et al. 2022).

IFS observations for the eCALIFA survey were carried out using the Potsdam MultiAperture Spectrophotometer (M. M. Roth et al. 2005) using the PPAK configuration (M. M. Roth et al. 2005) located at the 3.5 m telescope at the Calar Alto Observatory. The FoV of this instrument is $\sim 74'' \times 64''$ with spatial resolutions of $\sim 2\farcs5$. The eCALIFA survey adopted a low-resolution spectral configuration (V500, $R \sim 800$) with a large wavelength coverage (∼3700–7000 Å). Details regarding data reduction, instrumentation, and sample properties are explained in detail in S. F. Sánchez et al. (2012) and C. J. Walcher et al. (2014).

The final product of the observation for each galaxy is a data cube where the x- and y-axes correspond to the R.A. and decl. of the object, while the z-axis corresponds to the wavelength coverage. To determine maps of the physical properties for each of the galaxies in this survey, the data cube is analyzed using the analysis pipeline `PyPipe3D` (E. A. D. Lacerda et al. 2022), which is an updated version of the extensively used original `Pipe3D` pipeline (S. F. Sánchez et al. 2016b). In a nutshell, `PyPipe3D` is able to extract from optical data cubes maps of the physical properties related to both the stellar continuum and the emission lines from the ionized gas (e.g., J. K. Barrera-Ballesteros et al. 2016). One of the great advantages of having spatially resolved spectroscopic data is that it allows for comparisons between integrated measurements at different apertures (e.g., J. K. Barrera-Ballesteros et al. 2017; S. F. Sánchez et al. 2017, 2019).

For this study we use the maps of the stellar mass surface density, Σ_*; the star formation rate surface density derived from the single stellar-population (SSP) analysis, $\Sigma_{\rm SFR,SSP}$; the integrated flux of the Hα and Hβ emission lines; and the Hα line equivalent width, EW(Hα), measured at the effective radius ($R_{\rm eff}$). By adding up Σ_*, and $\Sigma_{\rm SFR,SSP}$ across the CALIFA FoV we estimate the integrated stellar mass and SFR from SSP analysis ($M_{*,\rm global}$, and $\rm SFR_{SSP}$). From the Hα and Hβ integrated fluxes we derive two quantities: the global star formation rate ($\rm SFR_{global}$), and the total molecular gas mass, $M_{\rm mol,Av}$. For the first, we convert the dust-corrected Hα luminosity to $\rm SFR_{global}$ using the calibrator derived by R. C. Kennicutt (1998) and assuming a E. E. Salpeter (1955) initial mass function whereas to estimate $M_{\rm mol,Av}$, we follow the calibrator derived by J. K. Barrera-Ballesteros et al. (2020). This calibrator compares the optical extinction derived from the Hα/Hβ ratio with the molecular gas mass (density) for integrated (and resolved) scales, thus $F_{\rm mol,global} = M_{\rm mol,Av}/M_{*,\rm global}$ and $\rm SFE_{global} = SFR_{global}/M_{mol,Av}$. We note that, on the one hand, the integrated flux of Hα and Hβ could be the result from the contribution of several physical process not related to star formation. Thanks to the nature of the CALIFA data set we test that for most of the galaxies considered as star forming (i.e., with EW(Hα)—measured at $R_{\rm eff}$—larger than 6 Å, see the details in Section 3) the spatially resolved emission correspond to star formation. In other words, we assure that the emission line ratios [N II]/Hα and [O III]/Hβ are below the L. J. Kewley et al. (2001) demarcation line in their corresponding diagnostic diagram. On

the other hand, we consider the limitations of using the optical extinction in order to derive the molecular mass discussed in J. K. Barrera-Ballesteros et al. (2020). In Section 4 we discuss how these caveats could have an impact on our main conclusions.

The optical spatially resolved information provided by the CALIFA survey has paved the way to explore how the physical parameters derived from the optical correlate with the amount of cold gas at kiloparsec scales. Some of these studies have been carried out within the EDGE-CALIFA survey (A. D. Bolatto et al. 2017), which provides spatially resolved measurements of the ^{12}CO and ^{13}CO emission lines for 125 CALIFA galaxies using the Combined Array for Millimeter-wave Astronomy interferometer. The EDGE-CALIFA survey has been essential to understand the intimate relation that different components of the baryonic mass have with the star formation activity at kiloparsec scales (e.g., D. Utomo et al. 2017; J. K. Barrera-Ballesteros et al. 2021b; S. F. Sánchez et al. 2021). Further efforts have also endeavored to have homogeneous observations of the ^{12}CO emission lines for a large sample of CALIFA galaxies. This is the case of the data set presented by D. Colombo et al. (2020). Together with synthetic integrated measurements (i.e., integrated measurements from the EDGE maps) from the EDGE-CALIFA CO data and APEX observations, they report single-aperture ^{12}CO(2–1) data for more than 470 CALIFA galaxies. APEX typical resolution or beam size is $\sim$26″ at 230 GHz, which corresponds roughly to 1 effective radius for this sample. However, the range of coverage of the beam goes from $\sim$0.5 to $\sim$2.5 effective radii measured in the r band. For this study we use an updated APEX sample comprising a total database of 633 observations for 572 galaxies, including off-center pointings. This database also provides some parameters derived from the optical CALIFA IFS integrated within the APEX beam size. For this study we are going to use the following parameters in the aforementioned data set: $\mathrm{SFR_{center}}$, and $M_{*,\mathrm{center}}$, as well as the parameters derived from the ^{12}CO observations such as $\mathrm{M_{mol,center}}$ (see D. Colombo et al. 2020 for details); thus, $F_{\mathrm{mol,center}} = M_{\mathrm{mol,center}}/M_{*,\mathrm{center}}$, and $\mathrm{SFE_{center}} = \mathrm{SFR_{center}}/M_{\mathrm{mol,center}}$.

In summary, from the APEX data set we select those galaxies with reliable CO central measurements, that is, those galaxies with central CO flux larger than $M_{\mathrm{mol}} \sim 0.4 \times 10^8 M_\odot$ (389 targets; D. Colombo et al. 2020; D. Colombo et al. 2024, in preparation). On the other hand, from the entire eCALIFA sample (823 galaxies) we use those galaxies with a reliable estimation of $M_{\mathrm{mol,Av}}$ (i.e., galaxies with integrated Hα/Hβ line ratios larger than 2.86 and an integrated Hα flux signal-to-noise ratio larger than 3). To emulate similar observational conditions as those from APEX we also select galaxies with $M_{\mathrm{mol,Av}} > 0.4 \times 10^8 M_\odot$ (468 galaxies). We note that selecting galaxies with this line ratio guarantees the reliable estimation of the molecular gas mass from optical extinction (see Figure 2 in J. K. Barrera-Ballesteros et al. 2020). The CALIFA data also allow us to provide a comparison between the central M_{mol} provided by the APEX observation and those derived using the central portion of the IFS data (see Figure 6). We find that, despite the scatter, both estimations show similar values of M_{mol}. Finally, we use the morphological classification provided by the database `HyperLeda`.[7]

[7] http://leda.univ-lyon1.fr/

3. Results

In Figure 1 we plot our sample of global and central measurements in the SFR–M_* plane (top and bottom panels, respectively). Following different studies, we consider star-forming (retired) galaxies (SFGs and RGs, respectively) as those with an EW(Hα)—measured at R_{eff}—larger (smaller) than 6 Å (e.g., E. A. D. Lacerda et al. 2022). For both set of measurements we perform a linear fit in logarithm scales only for star-forming galaxies (blue and green solid lines in Figure 1, respectively). These are our estimations of the SFMS for each set of measurements. In comparison to previous estimations of the SFMS, the one using the global measurements is very similar to the one derived using integrated measurements from a smaller sample of the CALIFA survey (red dashed line in Figure 1; M. Cano-Díaz et al. 2016). However, for the central measurements the slope of the SFMS is flatter in comparison to global and previous measurements. This is clearly an aperture effect: on the one hand, central measurements enclose less flux from both the continuum and the Hα emission line. On the other hand, for massive galaxies in particular, the global measurements include larger star formation than the central aperture. This analysis also indicates that those results of the SFMS using measurements other than global (e.g., central apertures) should be treated with caution as they can induce to different conclusions regarding the shape of the SFMS.

3.1. ΔSFMS versus F_{mol}

For each galaxy in Figure 1, we quantify ΔSFMS as the vertical distance between its observed SFR and the expected one from the best fits presented for global and central measurements ($\Delta\mathrm{SFMS_{global}}$ and $\Delta\mathrm{SFMS_{center}}$, respectively). In the left and center panels of Figure 2 we plot how ΔSFMS changes with respect to the gas fraction, F_{mol}, for these measurements, respectively. We derive confidence ellipses[8] for both the SFGs and RGs for each of the two measurements. For the global measurements we find a significant correlation between these two parameters in each population of galaxies: $\Delta\mathrm{SFMS_{global}}$ increases with $F_{\mathrm{mol,global}}$ (Spearman correlations coefficients $\rho = 0.65$, and 0.52, respectively). For both populations we find similar orientations for their confidence ellipses. The dynamical range of $F_{\mathrm{mol,global}}$ is 2 orders of magnitude for the CALIFA galaxies with the star-forming galaxies having $\sim$10% gas fraction and the retired galaxies having on average 1% molecular gas. On the other hand, for the central measurements we note that the confidence ellipse for the SFGs has a flatter orientation in comparison to the one derived for RGs, which has a steeper ellipse. The 1σ confidence ellipses overlap for the SFG and RG samples suggesting that at the center of some retired galaxies $F_{\mathrm{mol,center}}$ is similar to the SFG sample.

To provide a direct comparison between the global and central measurements, we plot together in the right panel of Figure 2 the 1σ confidence ellipses derived for each of these measurements. For SFGs we find that the ellipses for the global and central measurements are in a similar location in the ΔSFMS–F_{mol} diagram (blue and green ellipses, respectively). Although their orientation is similar and the mean value of

[8] The major and minor axes of the confidence ellipse represent the standard deviation for the distribution in each parameter. Thus, a confidence ellipse represents the possible correlation, or lack thereof, between two parameters.

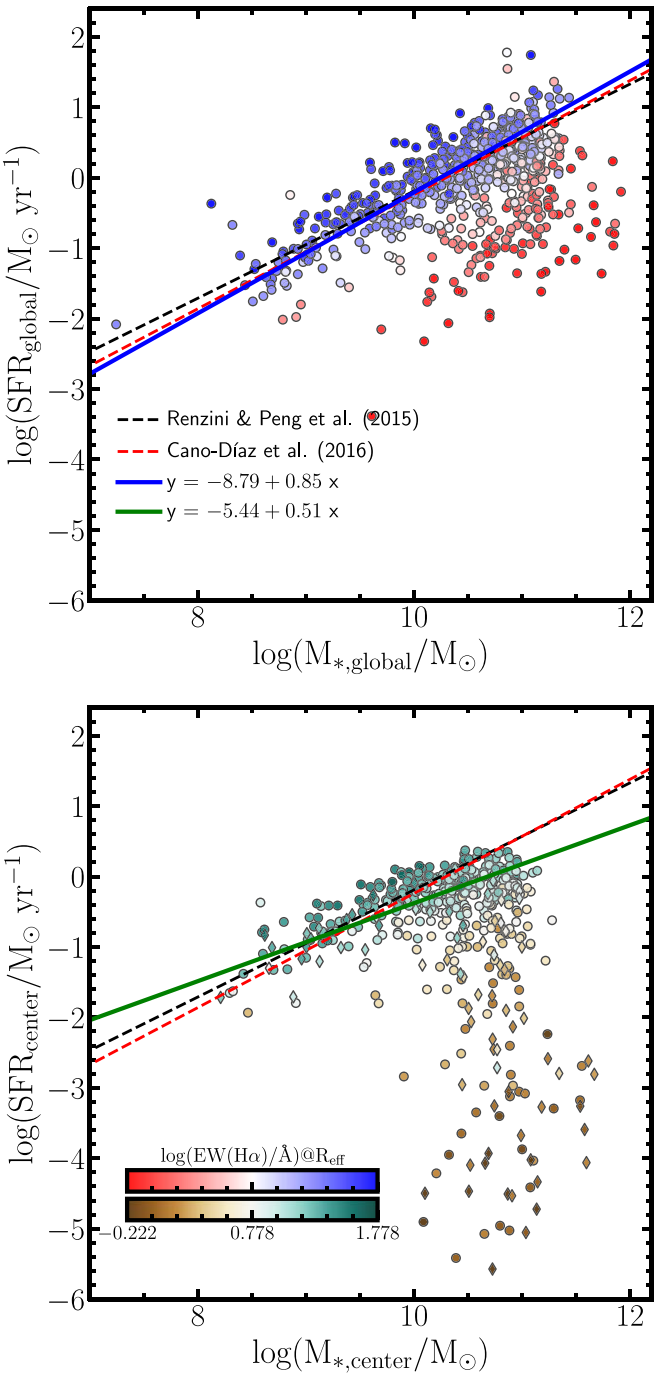

Figure 1. The global (top panel) and central (bottom panel) measurements of the SFR against the total stellar mass for the CALIFA and APEX-EDGE samples, respectively. Both are color coded by EW(Hα) measured at $R_{\rm eff}$—the color palettes simply differentiate global (red to blue) and central (yellow to green) measurements. The dashed black and red lines represent the best fits from previous estimations of the SFMS (A. Renzini & Y.-j. Peng 2015; M. Cano-Díaz et al. 2016, respectively). The blue (top) and green (bottom) solid lines represent the best fits from the SFMS using the global and central star formation measurements (i.e., the blue and green points), respectively. For a galaxy with a given M_*, we quantify ΔSFMS as the vertical distance between its observed SFR and the expected one from these best fits. The circle and diamond symbols in the bottom panel represent the measurements above and below the APEX detection limit, respectively.

ΔSFMS is close to zero, we find that $F_{\rm mol,global}$ covers a slightly larger dynamical range in comparison to $F_{\rm mol,center}$ with a slightly larger mean value of $F_{\rm mol}$. On the other hand for RGs, we find that the median value of ΔSFMS for the global measurements is significantly higher than the one from central measurements, with the mean value of $F_{\rm mol,center}$ being $\sim$0.3 dex larger in comparison to $F_{\rm mol,global}$ (marked as red and orange stars in the right panel of Figure 2, respectively). Furthermore, the orientation of the ellipses is different. In comparison to the global measurements, the confidence ellipse for central measurements is significantly steeper. Although both measurements share similar values of $F_{\rm mol}$ for small values of ΔSFMS, as the galaxies depart from the SFMS, the lack of molecular gas became significantly evident for global measurements in comparison to the central ones.

In comparison to the trends observed for the central measurements in retired galaxies, our results shows that the global gas fraction is smaller than the central gas fraction (for a given ΔSFMS). This suggests that for these retired galaxies the gas fraction is smaller in their outskirts in comparison to their centers; furthermore, this trend becomes more significant as the galaxies further depart from the SFMS.

3.2. ΔSFMS versus SFE

In Figure 3 we compare ΔSFMS with respect to the SFE for the global and central measurements (left and center panels, respectively). For the global measurements, we find that the SFGs exhibit a rather roundish confidence ellipse while the RGs show a significant correlation with the ΔSFMS decreasing as SFE decreases ($\rho = 0.55$). In comparison to the SFE values we derived for the SFGs, we find that the RGs exhibit similar efficiencies. This could suggest that for those RGs the global SFR is more efficient consuming the molecular gas available than SFGs. For SFGs we find that $\rm SFE_{global}$ covers a narrow dynamical range ($\rm SFE_{global} \sim 10^{-10}$–$10^{-8.5}\,yr^{-1}$). The confidence ellipse for the central measurements of the SFGs has a positive orientation, in other words, the orientation of the ellipse suggests that $\Delta\rm SFMS_{center}$ increases with $\rm SFE_{center}$ ($\rho = 0.92$). On the other hand, the retired galaxies cover a wide range of efficiencies. The orientation of the confidence ellipse for these galaxies highlights the significant correlation between $\Delta\rm SFMS_{center}$ and $\rm SFE_{center}$: ΔSFMS increases with SFE. We note that both SFGs and RGs show similar confidence ellipse orientations, with the first being slightly flatter than the second.

In the right panel of Figure 3 we compare the confidence ellipses for the SFGs and RGs using the global and central measurements. First, we note that for the SFGs the mean values of ΔSFMS are close to each other ($\sim$0 dex); however, the SFE is larger for global measurements in comparison to central ones. Even though the ellipses for both central and global measurements of the SFGs galaxies overlap, the median SFE for the global measurements is slightly larger than the one for the central regions. On the other hand, for the RGs, we find significant differences in both the ΔSFMS and SFE for the global and central measurements. The departure of the central measurements from the SFMS is steeper and larger in comparison to the global measurements. Furthermore, the SFE measured at global scales is larger in comparison to those derived at central scales. These results suggest that the efficiency of transforming gas into stars in retired galaxies is much larger in their outskirts than at their centers. Although these results are very intriguing, we take them with caution. In the next section we discuss the possible caveats of these results in terms of the sensitivity limits of the observed parameters.

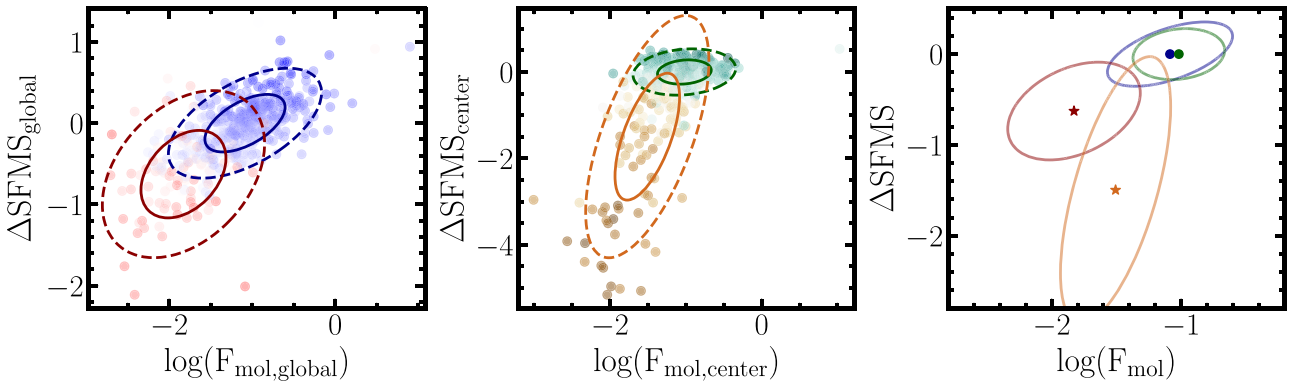

Figure 2. ΔSFMS against the gas fraction (F_{mol}) using two different apertures to estimate the physical properties. The left panel shows the comparison between these quantities using global properties ($\Delta SFMS_{global}$ vs. $F_{mol,global}$). The data points are color coded according to the EW(Hα) measured at their R_{eff}. The solid and dashed ellipses represent the 1σ and 2σ confidence levels of the distribution, respectively. Blue and red ellipses represent those confidence levels measured for star-forming and retired galaxies, respectively. The center panel shows a similar comparison for central properties ($\Delta SFMS_{center}$ vs. $F_{mol,center}$). Data points are also color coded according to the EW(Hα) measured at their R_{eff}. The orange and green ellipses represent similar fractions as in the left panel. The right panel shows the comparison between the 1σ ellipses for global and central measurements, while the stars represent the median values for star-forming and retired galaxies for each measurement, respectively.

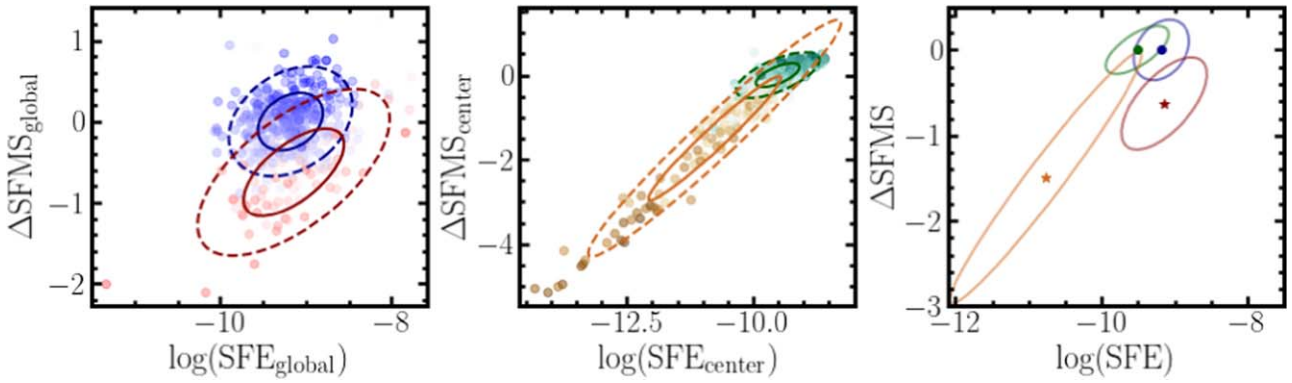

Figure 3. ΔSFMS against the star formation efficiency (SFE) using two different apertures to estimate the physical properties. The layout of the figure is similar to the one for Figure 2.

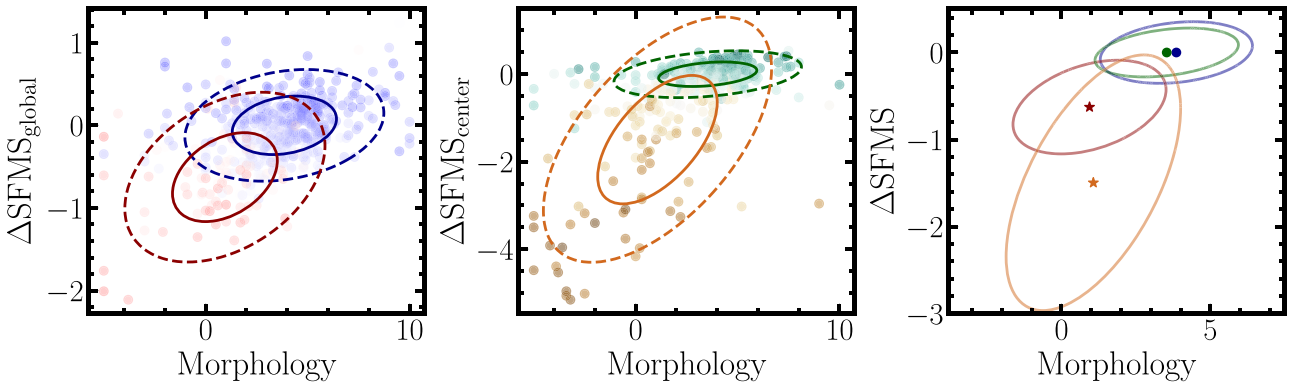

Figure 4. ΔSFMS against the morphology using two different apertures to estimate the physical properties. The layout of the figure is similar to the one for Figure 2.

3.3. ΔSFMS versus Morphology

Finally, we also want to explore the explicit relation between ΔSFMS with respect to the morphology from the global and central measurements (see the left and center panels of Figure 4, respectively). As we mention in Section 2, we follow the `HyperLeda` morphological classification scheme (de Vaucouleurs one) where values below 1 are associated with early-type galaxies, whereas late-type galaxies are assigned values larger than 1. For the global measurements, we find that SFGs show a rather mild correlation between $\Delta SFMS_{global}$ and the morphology. $\Delta SFMS_{global}$ tends to move from negative to positive values from values from 0 to 7 in morphology (i.e., from S0 to Sd types). On the other hand, RGs are associated with early-type galaxies (i.e., E/S0 types). For RGs we find a mild correlation between $\Delta SFMS_{global}$ and morphology in comparison to SFGs (as measured by the positive slope of the red confidence ellipses). In other words, elliptical galaxies are located farther away from the SFMS in comparison to the

lenticular galaxies. Similar to the global measurements, we find that for central measurements the SFGs also show a flat relation between their morphological type and $\Delta SFMS_{center}$. In other words, the central values of ΔSFMS remain relatively constant for SFGs regardless of their morphological type. This is not the case for retired galaxies, where we find that the residuals of the SFMS measured at their centers depart away from the best fit of this scaling relation as the galaxy moves from lenticular to earlier types.

Similar to the other explored properties (F_{mol} and SFE), for the sake of comparison we plot in the right panel of Figure 4 the confidence ellipses derived for the SFGs and RGs using the central and global measurements for different morphologies. For SFGs we note the remarkable similarity between the location of the median value of ΔSFMS and the average morphology (∼4; Sbc type) for both the global and central measurements (see blue and green filled circles, respectively) as well as the shape and orientations of their confidence ellipses (blue and green ellipses, respectively). On the other hand, although the median value of ΔSFMS for both measurements are similar (∼1.1 dex), the average value of morphology varies between the global and central measurements. Both global and local measurements show a median value close to 1 (lenticular galaxies). However, the median ΔSFMS of the central measurements is significantly smaller than those derived from the global measurements. The large dynamical range of ΔSFMS for the central measurements is also evident in comparison to the global ones. In other words, although central and global ΔSFMS are similar for the most late-type RGs as the ΔSFMS departs from the SFMS, $\Delta SFMS_{global}$ is measured in earlier-type galaxies in comparison to the same value of $\Delta SFMS_{center}$. Finally, we note that this behavior of ΔSFMS versus the morphology is similar to the one we derive between ΔSFMS and the gas fraction (see the right panel of Figure 2). This is expected given the well-known relation between the gas fraction and the morphology of galaxies, where F_{mol} for early-type galaxies is significantly smaller in comparison to late-type ones (e.g., A. Saintonge et al. 2017).

In summary, our results indicate that the physical properties (F_{mol} and SFE) at different scales (global and central) of the retired galaxies for a given SFR deficit—measured by the ΔSFMS—are significantly different. On the one hand, our results suggest that, in general, there is more gas located at the central part of these retired galaxies that in their outskirts. On the other hand, the SFE is larger for global measurements in comparison to their central counterparts. These results may imply a scenario in which the central molecular gas temperature and/or density in retired galaxies are not optimal to be transformed into new stars; however, the small amount of gas available in their outskirts is efficiently consumed in new star formation. In the next section we explore how the observables that we use could have an impact on the above results.

4. Discussion and Conclusions

Using the largest sample of galaxies with optical IFS and central molecular gas observations, the APEX-CALIFA sample (572 targets), we are able to quantify how the central and global variations of the SFR with respect to its expected value from the SFMS, ΔSFMS, is affected by the central and global gas fraction and SFE. We segregate our galaxy sample in SFGs and RGs using the EW(Hα) measured at the effective radius, assuming EW(Hα) > 6 Å as the threshold to select SFGs. Focusing mostly on the RG sample, we find significant differences between the central and global measurements in the ΔSFMS–F_{mol} and ΔSFMS–SFE planes (see Figures 2 and 3, respectively).

On the one hand, for the same value of ΔSFMS (in central and global measurements) $F_{mol,center}$ is larger in comparison to $F_{mol,global}$ (see Figure 2). On the other hand, for the same value of ΔSFMS SFE_{global} is significantly larger than SFE_{center} (see Figure 3). We find similar results to those derived in the ΔSFMS–F_{mol} plane than in the ΔSFMS–Morphology plane (see Figure 4). As we mention in the previous section, our results suggest that even though there is a large fraction of gas at the center of the retired galaxies, in comparison to their outskirts, this is not a necessary condition to have a large efficiency at the center of these galaxies. On the contrary, we find that the SFE is significantly larger for global measurements in comparison to central values. Below we mention how the parameters that we use can affect these conclusions.

As we mention in Section 2, although we use CO measurements to estimate F_{mol} at the central region from the APEX observations, in order to estimate the molecular gas at global scales we use the calibrator presented in J. K. Barrera-Ballesteros et al. (2020). As we mention in Section 2, this calibrator uses the optical extinction derived from the Hα/Hβ ratio to have an estimation of the molecular gas at both global (integrated) and spatially resolved scales. Since the estimations of the molecular gas are different for the central and global measurements, this could affect the main conclusions of our study. To explore the impact of the different estimations of F_{mol}, we derive $F_{mol,center}$ using the map of Σ_{mol} from the CALIFA data set and integrating over an aperture that simulates the beam size of the APEX observations. We find that using this estimation of the molecular gas provides similar results as those presented in the previous section when using the APEX data set. In J. K. Barrera-Ballesteros et al. (2020) we tested that the integrated global measurements of the molecular gas mass are similar when using either the optical extinction or the CO luminosity.

Another point to consider regarding our results is that we are assuming that the Hα luminosity of the entire galaxy corresponds to SFR. This may not be the case for RGs where the ionization source responsible for the Hα emission corresponds to other mechanisms than star formation (e.g., ionization by old stars, shocks, etc.; see S. F. Sánchez 2020, and references therein). Fortunately, the SSP analysis used to fit the stellar continuum allows us to have an estimation of the SFR. We use the integrated measurements of the SFR derived from the latest stellar population (∼32 Myr). As in the previous test, we find similar results as those derived in Section 3 using the Hα luminosity as a proxy of the SFR. Although at kiloparsec scales the SFR derived from the SSP analysis is similar to the one derived from the Hα luminosity for star-forming galaxies (e.g., J. K. Barrera-Ballesteros et al. 2021a), we confirm this is also the case when using integrated global properties for the CALIFA sample.

Different studies have explored the role of both the molecular gas and the SFE in the quenching of star formation rate. Using the APEX-CALIFA data set (a slightly smaller sample as the one used in this study), D. Colombo et al. (2020) found that the deficit of the global SFR (i.e., larger negative values of $\Delta SFMS_{global}$) correlates with a deficit of both the central F_{mol} and SFE. Their results are in agreement with previous studies using aperture-limited integrated properties that point to the paramount role that both the deficit of F_{mol} and SFE have in setting the SFR of an RG

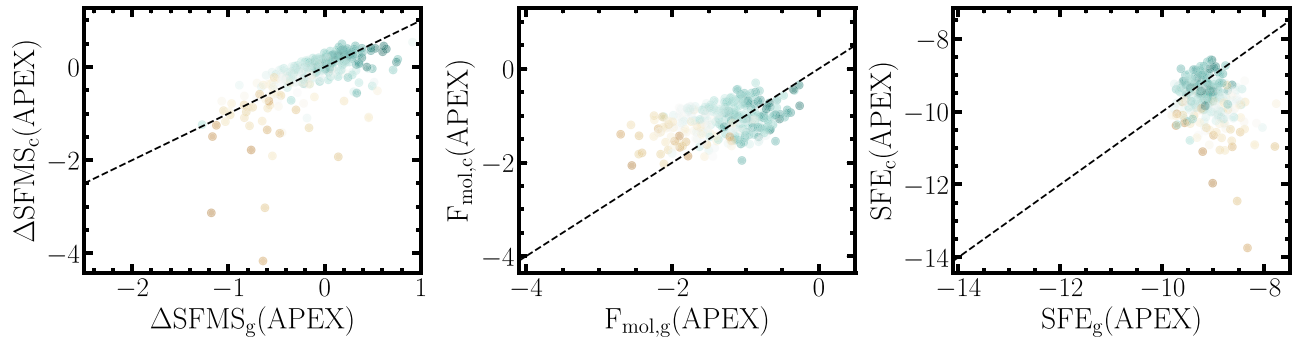

Figure 5. Comparison between the central and global parameters ΔSFMS, F_{mol}, and SFE in the left, center, and right panels, respectively, used in this study for the APEX sample (389 galaxies). The points are color coded according to the EW(Hα) measured at R_{eff} (>6 Å for SFGs). In all panels the dashed lines represent a one-to-one relation. These comparisons agree with the results we derive using the entire CALIFA sample in Section 3.

away from the SFMS (A. Saintonge et al. 2012, 2016, 2017). As expected, for the central measurements our results are in excellent agreement with those derived by D. Colombo et al. (2020, i.e., the median values of ΔSFMS, F_{mol}, and SFE are similar as well to the orientations of the confidence ellipses in the center panels of Figures 2 and 3). However, the relations we derive from global measurements differ in comparison to those obtained in the central regions. The fact that we are not using the same sample to estimate the central and global properties could indeed affect the conclusions of this study. Fortunately, as we mention above, the galaxies with central CO measurements are included in the CALIFA survey; therefore, we can also explore how the different parameters derived in this study vary from global to central measurements. In Figure 5 we compare the residuals of the SFMS, the gas fraction, and the SFE for the central and global measurements only for the galaxies with APEX observations (left, center, and right panels, respectively). First, we observe that for SFGs, ΔSFMS is similar for central and global measurements. However, for galaxies with EW(Hα) < 6 Å (i.e., RGs), the central deficit of ΔSFMS significantly drops in comparison to observed global values (reaching for some galaxies differences of ∼3 dex). This is evidence that the deficit of star formation in retired galaxies occur in an "inside-out" fashion (e.g., R. M. González Delgado et al. 2014; V. Kalinova et al. 2021). On the other hand, as we mention in the previous section (see the right panel of Figure 2), F_{mol} is larger at the center of RGs in comparison to the global measurements (see the center panel of Figure 5). This is another piece of evidence that the gas fraction at the center for RGs is larger in comparison to their outskirts. Finally, we corroborate our results using the entire CALIFA sample (see the right panel of Figure 3), that is, that the SFE at the center of RGs is significantly smaller in comparison to those derived at global scales. Beyond confirming the results presented by D. Colombo et al. (2020), we are able to quantify the significant difference between central and global measurements of both the gas fraction and the SFE.

These results evidently imply a radial variation of the quenching in retired galaxies. Thus, spatially resolved measurements are significantly valuable to further constrain the observed trends. Indeed, different recent studies have explored the correlation of the deficit of star formation rate in comparison to F_{mol} and SFE at radial scales with mixed results. On the one hand, using a sample of 34 MaNGA galaxies with ALMA observations,[9] which include SF and green valley targets (S. L. Ellison et al. 2020), found that local variations of the resolved SFMS (i.e., Σ_{SFR} versus Σ_*) are more closely related to SFE than the gas fraction. However, using a similar analysis with a larger sample of galaxies, in S. F. Sánchez et al. (2021) we find that the residuals for SFGs do not have a physical, but statistical, origin. On the other hand, focusing only on a sample of seven green valley galaxies with MaNGA and ALMA observations, S. Brownson et al. (2020) found that both the gas fraction and the SFE measured at kiloparsec scales could be equally important in setting the quenching state at kiloparsec scales. With a sample of five galaxies, but a better spatial resolution than the aforementioned studies, L. Morselli et al. (2020) found that the gas fraction is the main driver to set the distance of a region away from the resolved SFMS rather than the SFE at subkiloparsec scales. Although spatially resolved studies are required to truly understand the main parameters that drive the radial quenching of galaxies, they lack a statistically robust sample that confidently traces the demographics of the galaxy population in the nearby Universe. We consider that studies as the one presented here are a first exploratory step to understand the spatially resolved quenching of galaxies (672 and 389 galaxies with global and central measurements, respectively).

As a whole, our results confirm that the quenching stage of a retired galaxy, measured by its distance away from the SFMS, ΔSFMS, interpreted as star formation deficit, correlates with both the gas fraction and the SFE. Beyond this, we are also able to quantify how those correlations of the SFR deficit with the gas fraction F_{mol} and the SFE vary depending on the aperture (central versus global). We confirm the so-called "inside-out" quenching, that is, that ΔSFMS is larger at the center of galaxies in comparison to the global measurement.

Furthermore, our results show that even though ΔSFMS is larger at their center (i.e., larger deficit), the central gas fraction in retired galaxies is larger in comparison to the global one. However, the global SFE is significantly larger in comparison to the central measurements. From this analysis we infer that instead of the lack of molecular gas, the deficit of ΔSFMS is related to the inefficiency of forming new stars, perhaps due to inadequate temperature and/or density, in the central regions of these galaxies, in contrast to their outskirts, which are more efficient. Given the correlations found between ΔSFMS and the morphology (see Figure 4), we suggest that structural parameters such as bulges at the center of early-type galaxies halt the conversion (or efficiency) from molecular gas to newly formed stars. In other words, although there is raw available material to form new stars in the central regions of galaxies,

[9] The ALMA-MaNGA QUEnching and Star-forming (ALMaQUEST) survey.

due to the formation of a spheroid or a bulge, this material is not able to dynamically cool off to collapse in order to form new stars (M. Martig et al. 2009), i.e., the bulge inhibits star formation. In the outskirts of these galaxies, although there is a deficit of molecular gas, their physical conditions are such that the efficiency is significantly large enough to have some ongoing star formation at global scales. In this scenario, lenticular and early spirals could have large gas fractions at their center, but the star formation is more efficient and occurs mostly at their outskirts (e.g., E. J. Johnston et al. 2017; J. Mendez-Abreu et al. 2019, 2021).

Acknowledgments

J.B.-B. acknowledges support from the grant IA-101522 (DGAPA-PAPIIT, UNAM) and funding from the CONACYT grant CF19-39578. I.C.G. acknowledges support from DGAPA-UNAM grant IN113320. R.C.L. acknowledges support for this work provided by a National Science Foundation (NSF) Astronomy and Astrophysics Postdoctoral Fellowship under award AST-2102625. This work was funded in part by NSF AAG grants 2307440 to the University of Illinois, and 2307441 to the University of Maryland.

Appendix
Central Molecular Gas Comparison

In Section 3 we use two estimations of $M_{\rm mol}$ for two different apertures, the one derived from APEX observations for the central region and the one derived from the optical extinction for the global or integrated measurements. In J. K. Barrera-Ballesteros et al. (2020) we showed that the integrated measurements from the optical extinction trace well those derived from CO (see their Figure 3). Thanks to the APEX central observation, in this study we are allow to compare how the central measurements using these two observables compare with each other. In Figure 6 we compare the central measurements derived from APEX observations and those derived using the optical extinction and the calibrator presented in J. K. Barrera-Ballesteros et al. (2020). We find that indeed both measurements are consistent with each other, both follow a one-to-one line (dashed line), for several orders of magnitude (Pearson correlation coefficient of $\rho \sim 0.6$). We also find that the median of the ratio between these two quantities ($\Delta M_{\rm mol}$; see the inset in Figure 6) is close to zero (~ -0.01 dex). Despite this, we also have to acknowledge that the scatter between these two measurements is large with a standard deviation of $\Delta M_{\rm mol}$ close to 0.7 dex. Our analysis shows that even tough these two measurements are similar the scatter is significant.

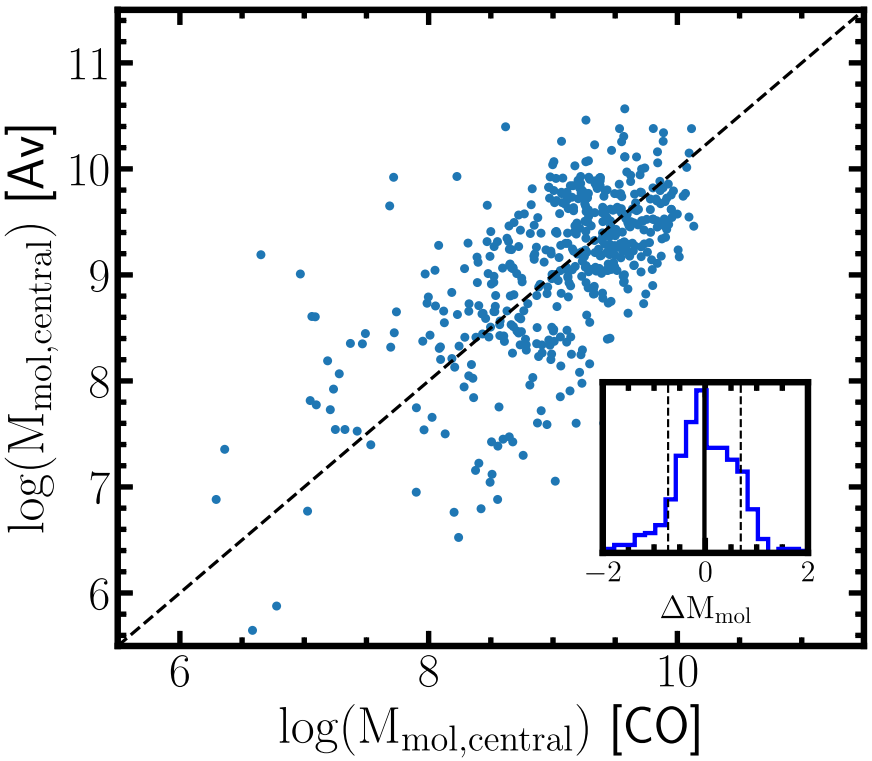

Figure 6. Comparison between the estimations of the molecular gas mass in the central area for the APEX sample (389 galaxies). The dashed line shows the one-to-one relation. The inset shows the histogram of the ratio in logarithm scale between these two measurements ($\Delta M_{\rm mol}$). Within the inset we show the median of $\Delta M_{\rm mol}$ (vertical solid black line) as well as the standard deviation of the sample (vertical dashed lines). Albeit there is scatter, the estimation of molecular gas from both measurements is similar.

ORCID iDs

J. K. Barrera-Ballesteros https://orcid.org/0000-0003-2405-7258
I. Cruz-González https://orcid.org/0000-0002-2653-1120
R. C. Levy https://orcid.org/0000-0003-2508-2586

References

Alatalo, K., Davis, T. A., Bureau, M., et al. 2013, MNRAS, 432, 1796
Alvarez-Hurtado, P., Barrera-Ballesteros, J. K., Sánchez, S. F., et al. 2022, ApJ, 929, 47
Barrera-Ballesteros, J. K., Heckman, T., Sánchez, S. F., et al. 2021a, ApJ, 909, 131
Barrera-Ballesteros, J. K., Heckman, T. M., Zhu, G. B., et al. 2016, MNRAS, 463, 2513
Barrera-Ballesteros, J. K., Sánchez, S. F., Heckman, T., & Blanc, G. A. 2017, ApJ, 844, 80
Barrera-Ballesteros, J. K., Sánchez, S. F., Heckman, T., et al. 2021b, MNRAS, 503, 3643
Barrera-Ballesteros, J. K., Utomo, D., Bolatto, A. D., et al. 2020, MNRAS, 492, 2651
Bell, E. F., van der Wel, A., Papovich, C., et al. 2012, ApJ, 753, 167
Bluck, A. F. L., Bottrell, C., Teimoorinia, H., et al. 2019, MNRAS, 485, 666
Bluck, A. F. L., Mendel, J. T., Ellison, S. L., et al. 2014, MNRAS, 441, 599
Bluck, A. F. L., Mendel, J. T., Ellison, S. L., et al. 2016, MNRAS, 462, 2559
Bolatto, A. D., Wong, T., Utomo, D., et al. 2017, ApJ, 846, 159
Breda, I., Papaderos, P., Gomes, J. M., et al. 2020, A&A, 635, A177
Brinchmann, J., Charlot, S., White, S. D. M., et al. 2004, MNRAS, 351, 1151
Brownson, S., Belfiore, F., Maiolino, R., Lin, L., & Carniani, S. 2020, MNRAS, 498, L66
Cameron, E., Driver, S. P., Graham, A. W., & Liske, J. 2009, ApJ, 699, 105
Cano-Díaz, M., Sánchez, S. F., Zibetti, S., et al. 2016, ApJL, 821, L26
Catalán-Torrecilla, C., Gil de Paz, A., Castillo-Morales, A., et al. 2017, ApJ, 848, 87
Colombo, D., Sánchez, S. F., Bolatto, A. D., et al. 2020, A&A, 644, A97
de Jong, R. S., & van der Kruit, P. C. 1994, A&AS, 106, 451
Dekel, A., & Silk, J. 1986, ApJ, 303, 39
Díaz-García, S., & Knapen, J. H. 2020, A&A, 635, A197
Ellison, S. L., Thorp, M. D., Lin, L., et al. 2020, MNRAS, 493, L39
García-Benito, R., Zibetti, S., Sánchez, S. F., et al. 2015, A&A, 576, A135
González Delgado, R. M., Pérez, E., Cid Fernandes, R., et al. 2014, A&A, 562, A47
Johnston, E. J., Häußler, B., Aragón-Salamanca, A., et al. 2017, MNRAS, 465, 2317
Kalinova, V., Colombo, D., Sánchez, S. F., et al. 2021, A&A, 648, A64
Kennicutt, R. C., Jr. 1998, ApJ, 498, 541
Kewley, L. J., Dopita, M. A., Sutherland, R. S., Heisler, C. A., & Trevena, J. 2001, ApJ, 556, 121
Lacerda, E. A. D., Sánchez, S. F., Cid Fernandes, R., et al. 2020, MNRAS, 492, 3073
Lacerda, E. A. D., Sánchez, S. F., Mejía-Narváez, A., et al. 2022, NewA, 97, 101895
Lang, P., Wuyts, S., Somerville, R. S., et al. 2014, ApJ, 788, 11
Leroy, A. K., Walter, F., Brinks, E., et al. 2008, AJ, 136, 2782
Liu, C., Hao, L., Wang, H., & Yang, X. 2019, ApJ, 878, 69
Martig, M., Bournaud, F., Teyssier, R., & Dekel, A. 2009, ApJ, 707, 250
Mendez-Abreu, J., de Lorenzo-Caceres, A., & Sánchez, S. F. 2021, MNRAS, 504, 3058
Mendez-Abreu, J., Sánchez, S. F., & de Lorenzo-Caceres, A. 2019, MNRAS, 484, 4298
Morselli, L., Rodighiero, G., Enia, A., et al. 2020, MNRAS, 496, 4606
Omand, C. M. B., Balogh, M. L., & Poggianti, B. M. 2014, MNRAS, 440, 843
Renzini, A., & Peng, Y.-j. 2015, ApJL, 801, L29
Roth, M. M., Kelz, A., Fechner, T., et al. 2005, PASP, 117, 620
Saintonge, A., Catinella, B., Cortese, L., et al. 2016, MNRAS, 462, 1749
Saintonge, A., Catinella, B., Tacconi, L. J., et al. 2017, ApJS, 233, 22
Saintonge, A., Tacconi, L. J., Fabello, S., et al. 2012, ApJ, 758, 73
Salpeter, E. E. 1955, ApJ, 121, 161
Sánchez, S. F. 2020, ARA&A, 58, 99
Sánchez, S. F., Barrera-Ballesteros, J. K., Colombo, D., et al. 2021, MNRAS, 503, 1615
Sánchez, S. F., Barrera-Ballesteros, J. K., López-Cobá, C., et al. 2019, MNRAS, 484, 3042
Sánchez, S. F., Barrera-Ballesteros, J. K., Sanchez-Menguiano, L., et al. 2017, MNRAS, 469, 2121
Sánchez, S. F., García-Benito, R., Zibetti, S., et al. 2016a, A&A, 594, A36
Sánchez, S. F., Kennicutt, R. C., Gil de Paz, A., et al. 2012, A&A, 538, A8
Sánchez, S. F., Pérez, E., Sánchez-Blázquez, P., et al. 2016b, RMxAA, 52, 21
Utomo, D., Bolatto, A. D., Wong, T., et al. 2017, ApJ, 849, 26
Veilleux, S., Maiolino, R., Bolatto, A. D., & Aalto, S. 2020, A&ARv, 28, 2
Veilleux, S., Meléndez, M., Sturm, E., et al. 2013, ApJ, 776, 27
Walcher, C. J., Wisotzki, L., Bekeraité, S., et al. 2014, A&A, 569, A1
Whitaker, K. E., Williams, C. C., Mowla, L., et al. 2021, Natur, 597, 485
Zibetti, S., Gallazzi, A. R., Ascasibar, Y., et al. 2017, MNRAS, 468, 1902